CHAPTER 21

Improved Boundary Conditions to a Time–Dependent Mild–Slope Equation for Random Waves

Toshimasa Ishii[1], Masahiko Isobe[2], and Akira Watanabe[2]

Abstract

The offshore and side boundary conditions to a time–dependent mild slope equation for random waves are improved to introduce given incident waves into and extract reflected waves from the computational domain with reduced computational time and storage size. The resulting numerical model is applied to calculate the wave field, nearshore current, and bottom topography change around a detached breakwater.

1   Introduction

A time–dependent mild–slope equation for random waves was derived from the mild slope equation by approximating frequency–independent expressions to the frequency–dependent coefficients (Kubo *et al.*, 1991; Kotake *et al.*, 1992). In the numerical solution, however, the peripheral region for absorbing the outgoing wave energy becomes large in comparison with the calculation domain of interest. In addition, because the velocity potential due to the incident waves must be calculated at each point in the peripheral region, extensive computational time is required.

The present study deals with the incident wave boundary condition and the open boundary condition in more detail and improves them, so that the deformation of multi–directional irregular waves may be calculated with much less computational time and storage size. The numerical model developed is applied to calculate the wave field, nearshore current, and bottom topography change around a detached breakwater on a uniform slope.

---

[1]Tokyo Electric Power Co., Ltd.
[2]Dept. of Civil Eng., Univ. of Tokyo, Bunkyo–ku, Tokyo 113, Japan

2   A time–dependent mild–slope equation for random waves

A time–dependent mild–slope equation for random waves (Kubo *et al.*, 1992) is given by

$$\nabla(\bar{\alpha}\nabla\tilde{\eta}) + i\nabla\left[\bar{\beta}\nabla\left(\frac{\partial\tilde{\eta}}{\partial t}\right)\right] + \bar{k}^2\bar{\alpha}(1 + if_D)\tilde{\eta} + i\bar{\gamma}(1 + if_D)\frac{\partial\tilde{\eta}}{\partial t} = 0 \qquad (1)$$

$$\bar{\alpha} = \bar{C}\bar{C}_g \qquad (2)$$

$$\bar{\beta} = \frac{\bar{C}}{\bar{k}}[-2(1 - \bar{n}) + \frac{1}{2\bar{n}}(2\bar{n} - 1)\{1 - (2\bar{n} - 1)\cosh 2\bar{k}d\}] \qquad (3)$$

$$\bar{\gamma} = \bar{k}\bar{C}[2\bar{n} + \frac{1}{2\bar{n}}(2\bar{n} - 1)\{1 - (2\bar{n} - 1)\cosh 2\bar{k}d\}] \qquad (4)$$

$$\bar{n} = (1/2)(1 + 2\bar{k}d/\sinh 2\bar{k}d) \qquad (5)$$

where $\bar{C}$ is the wave celerity, $\bar{C}_g$ the group velocity, $\bar{k}$ the wave number, d the water depth, t the time, ∇ the horizontal gradient operator, i the unit of imaginary number, and f_D an energy absorbing coefficient. The symbol $\overline{}$ denotes quantities at the representative frequency $\bar{\omega}$. The relation between $\tilde{\eta}$ and the temporal water surface variation η is :

$$\eta = Re[\tilde{\eta}e^{-i\bar{\omega}t}] \qquad (6)$$

3   Improvement of boundary condition for incident waves

3.1   Layer boundary method

In the numerical solution of horizontal two–dimensional problems, we introduce the incident waves at the offshore and side boundaries. In addition, the outgoing waves should propagate out at the boundaries without reflection.

Kubo *et al.* (1992) presented a method that satisfies the above conditions, whereby the incident waves are introduced through a layer boundary. This technique is illustrated in Figure 1. The energy of the outgoing waves is absorbed in the energy absorbing layer of a sufficient width, and the incident irregular waves must be prescribed as an excitation force at all grid points in the layer by a superposition of component waves. Consequently, the method requires considerable computational time and large storage, and therefore the number of component waves is restricted to about 200. Also, as seen from results of computations

performed by Kubo *et al.* (1992) and the authors for multi–directional irregular waves around a detached breakwater, the distribution of the wave height was asymmetrical due to the statistical variation.
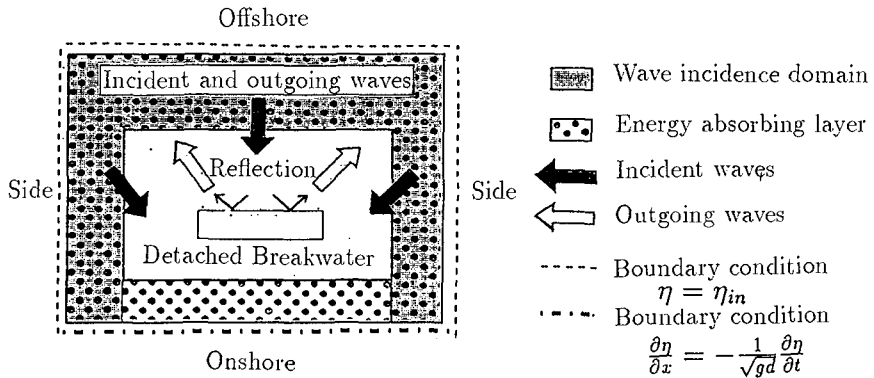
Offshore

Fig.1: Method for introducing incident waves through a layer boundary (Kubo *et al.*, 1992)

3.2   Line boundary method

The incident wave boundary condition is improved in the present study by introducing the incident waves through a line boundary as shown in Figure 2. The incident wave potential is only specified along the line boundary, which significantly reduces computational time and storage. With the new method wave transformation can be calculated for irregular incident waves even with as many as 1,000 components, whereas the previous method has a practical limit of about 200 components. As a result, the deformation of multi–directional irregular waves can be calculated with a much higher accuracy because the statistical variation is reduced.

The method is summarized in the following. First we set up a line boundary where the incident waves are introduced. Inside the line boundary, incident and outgoing waves are to be dealt with, whereas only outgoing waves exist outside the line boundary as shown in Figure 2. For this purpose, we only have to adjust the incident wave component $\tilde{\eta}_{in}$ in the finite difference equation for which the central grid point is located adjacent to the line boundary. The incident waves are introduced into the calculation domain through this operation.
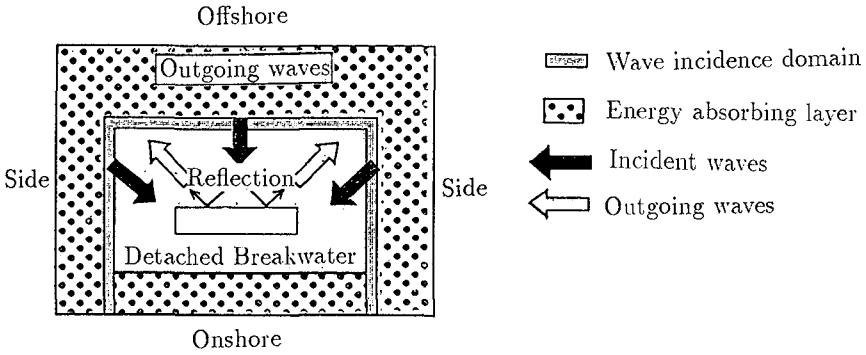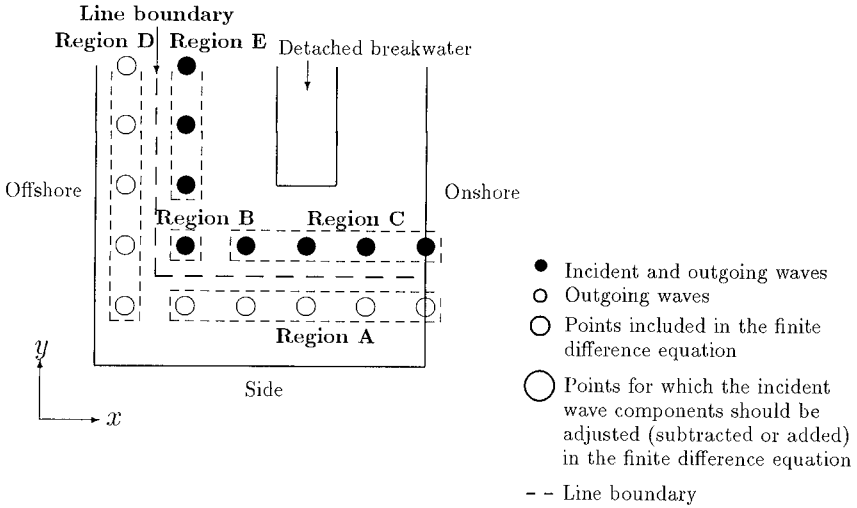
Offshore

Onshore

Fig.2: Method for introducing incident waves through a line boundary

To describe the method in more detail, we apply it to a horizontal two–dimensional problem. The ADI method is employed in the numerical calculations to solve the present equation. The calculations are carried out alternately in the x and y directions, implying that the application of the present method must be considered separately for each direction. Figure 3 shows the application in the x direction. For a horizontal two–dimensional model on a uniform slope, the finite difference equation of the time–dependent mild–slope equation for random waves in the x direction is written

$$
\frac{\bar{\alpha}_{i+1} - \bar{\alpha}_{i-1}}{2\Delta x} \left\{ \frac{\tilde{\eta}_{i+1,j}^{t+1} - \tilde{\eta}_{i-1,j}^{t+1}}{2\Delta x} \right\}
$$

$$
+ \ \bar{\alpha}_i \left\{ \frac{\tilde{\eta}_{i-1,j}^{t+1} - 2\tilde{\eta}_{i,j}^{t+1} + \tilde{\eta}_{i+1,j}^{t+1}}{\Delta x^2} + \frac{\tilde{\eta}_{i,j-1}^{t} - 2\tilde{\eta}_{i,j}^{t} + \tilde{\eta}_{i,j+1}^{t}}{\Delta y^2} \right\}
$$

$$
+ \ i\frac{\bar{\beta}_{i+1} - \bar{\beta}_{i-1}}{2\Delta x} \left\{ \frac{(\tilde{\eta}_{i+1,j}^{t+1} - \tilde{\eta}_{i-1,j}^{t+1}) - (\tilde{\eta}_{i+1,j}^{t} - \tilde{\eta}_{i-1,j}^{t})}{2\Delta x \Delta t} \right\}
$$

$$
+ \ i\bar{\beta}_i \left\{ \frac{(\tilde{\eta}_{i-1,j}^{t+1} - 2\tilde{\eta}_{i,j}^{t+1} + \tilde{\eta}_{i+1,j}^{t+1}) - (\tilde{\eta}_{i-1,j}^{t} - 2\tilde{\eta}_{i,j}^{t} + \tilde{\eta}_{i+1,j}^{t})}{\Delta x^2 \Delta t} \right.
$$

$$
+ \ \left. \frac{(\tilde{\eta}_{i,j-1}^{t} - 2\tilde{\eta}_{i,j}^{t} + \tilde{\eta}_{i,j+1}^{t}) - (\tilde{\eta}_{i,j-1}^{t-1} - 2\tilde{\eta}_{i,j}^{t-1} + \tilde{\eta}_{i,j+1}^{t-1})}{\Delta y^2 \Delta t} \right\}
$$

$$
+ \ \bar{k}^2 \bar{\alpha}_i (1 + if_D) \frac{\tilde{\eta}_{i,j}^{t+1} + \tilde{\eta}_{i,j}^{t}}{2} + i\bar{\gamma}_i (1 + if_D) \frac{\tilde{\eta}_{i,j}^{t+1} - \tilde{\eta}_{i,j}^{t}}{\Delta t} = 0 \qquad (7)
$$

By rearranging the equation under the condition that $\Delta x = \Delta y = \Delta l$, the left–hand side contains only unknown values (time step $t+1$) and the right–hand side

Line boundary

Region D | Region E   Detached breakwater

Offshore   Onshore

Region B   Region C

Region A

Side

y

x

- ● Incident and outgoing waves
- ○ Outgoing waves
- ⊙ Points included in the finite difference equation
- ⬭ Points for which the incident wave components should be adjusted (subtracted or added) in the finite difference equation
- – – Line boundary

	Region A	Region B	Region C	Region D	Region E
t+1 Step	No operation	$+\tilde{\eta}_{i-1,j,in}^{t+1}$	No operation	$-\tilde{\eta}_{i+1,j,in}^{t+1}$	$+\tilde{\eta}_{i-1,j,in}^{t+1}$
t Step	$-\tilde{\eta}_{i,j+1,in}^{t}$	$+\tilde{\eta}_{i-1,j,in}^{t}+\tilde{\eta}_{i,j-1,in}^{t}$	$+\tilde{\eta}_{i,j-1,in}^{t}$	$-\tilde{\eta}_{i+1,j,in}^{t}$	$+\tilde{\eta}_{i-1,j,in}^{t}$
t-1 Step	$-\tilde{\eta}_{i,j+1,in}^{t-1}$	$+\tilde{\eta}_{i,j-1,in}^{t-1}$	$+\tilde{\eta}_{i,j-1,in}^{t-1}$	No operation	No operation

Fig.3: Illustration of the method of introducing incident waves through a line boundary for the case of calculation in the x direction

only known values (time steps t and $t-1$), and the above equation can be written

$$A1_i\tilde{\eta}_{i-1,j}^{t+1} + A2_i\tilde{\eta}_{i,j}^{t+1} + A3_i\tilde{\eta}_{i+1,j}^{t+1}$$
$$= B1_i\tilde{\eta}_{i-1,j}^{t} + B2_i\tilde{\eta}_{i,j}^{t} + B3_i\tilde{\eta}_{i+1,j}^{t} + B4_i\tilde{\eta}_{i,j-1}^{t} + B5_i\tilde{\eta}_{i,j+1}^{t}$$
$$+ C1_i\tilde{\eta}_{i,j-1}^{t-1} + C2_i\tilde{\eta}_{i,j}^{t-1} + C3_i\tilde{\eta}_{i,j+1}^{t-1} \tag{8}$$

where (i, j) is the grid number in the (x, y) coordinate system, t the time,

$A1_i \sim A3_i$, $B1_i \sim B5_i$ and $C1_i \sim C3_i$ the coefficients determined by $\bar{\alpha}_i, \ddot{\beta}_i, \bar{\gamma}_i$ etc. Equation (8) includes grid points indicated with a double circle in Figure 3. There are three such points at time $t+1$, five points at time t and three points at time $t-1$ around the central grid point (i, j). These grid points are divided into two types according to their position relative to the line boundary. In the first type incident and outgoing waves coexist, and these grid points are shown with solid circles. In the second type only outgoing waves exist, which is indicated by empty circles. As an illustration, let us consider region A. The point$(i, j+1)$ at times t and $t-1$ are points including both incident and outgoing waves whereas the double circle points are points with outgoing waves only. Hence, we apply an operation which subtracts the incident wave term $\tilde{\eta}^t_{i,j+1,\mathrm{in}}$, $\tilde{\eta}^{t-1}_{i,j+1,\mathrm{in}}$ from point$(i, j+1)$ at times t and $t-1$. For this particular case, the finite difference equation (8) applied to outgoing waves may be written

$$
\begin{aligned}
& A1_i\tilde{\eta}^{t+1}_{i-1,j} + A2_i\tilde{\eta}^{t+1}_{i,j} + A3_i\tilde{\eta}^{t+1}_{i+1,j} \\
=\ & B1_i\tilde{\eta}^t_{i-1,j} + B2_i\tilde{\eta}^t_{i,j} + B3_i\tilde{\eta}^t_{i+1,j} + B4_i\tilde{\eta}^t_{i,j-1} + B5_i\tilde{\eta}^t_{i,j+1} \\
& + C1_i\tilde{\eta}^{t-1}_{i,j-1} + C2_i\tilde{\eta}^{t-1}_{i,j} + C3_i\tilde{\eta}^{t-1}_{i,j+1} \\
& - B5_i\tilde{\eta}^t_{i,j+1,\mathrm{in}} - C3_i\tilde{\eta}^{t-1}_{i,j+1,\mathrm{in}}
\end{aligned}
\tag{9}
$$

In regions B to E, the incident waves are introduced along the line boundary using the same method. In the case of the y direction, the position of the double circles at $t+1$ and $t-1$ time step should be reversed.

The computational time required by the present method was compared with the previous method for the case of a calculation region with 80×100 grid points, 100 component waves, and 3000 time steps. Multi–directional irregular waves were expressed using the single summation method. In this case, the computational time required by the present method was one–third that of the previous method.

4 Improvement of open boundary condition

4.1 One–dimensional open boundary condition

The boundary condition at the outer edge of the energy absorbing layer used in the numerical calculations presented by Kubo *et al.* (1992) is shown in Figure 1. The one–dimensional Sommerfeld radiation condition is employed at the onshore boundary with the celerity C approximated by the long wave celerity in the same way as Ohyama *et al.* (1990). This condition is motivated by the fact that the wave direction becomes perpendicular to the onshore boundary due to wave refraction. The condition at the offshore and side boundary is that the water

surface elevation is equal to that of the incident waves. This condition is based on the assumption that the outgoing waves are absorbed perfectly in the energy absorbing layer. In the numerical calculation presented by Kubo *et al.* (1992), a wide energy absorbing layer was needed to achieve perfect absorption.

In the present study, a new open boundary condition is derived from the Sommerfeld–type boundary condition by applying a Taylor expansion in terms of the angular frequency and wave direction. The aim is to reduce the energy absorbing layer. We present the result for the one–dimensional case first and then for the two–dimensional case.

The new open boundary condition for the one–dimensional case may be written

$$\eta(x_b, t + \Delta t) = \eta(x_b - \bar{C}\Delta t, t)$$
$$+ \bar{C}(1 - \bar{n})\Delta t [\frac{\partial \eta(x_b - \bar{C}\Delta t, t)}{\partial x} - i\bar{k}\eta(x_b - \bar{C}\Delta t, t)] \tag{10}$$

where $\eta(x_b, t + \Delta t)$ is the water surface elevation at the outer edge of the energy absorbing layer, and $\bar{C}$, $\bar{n}$ and $\bar{k}$ the wave celerity, shallowness factor and wave number at the representative frequency, respectively.

Equation(10) consists of coefficients which are independent of the frequency of component waves as a result of applying the Taylor expansion to the wave celerity C, which is a coefficient in the Sommerfeld–type boundary condition. Equation (10) is, therefore, applicable to irregular waves. The physical meaning of equation (10) is illustrated in Figure 4.
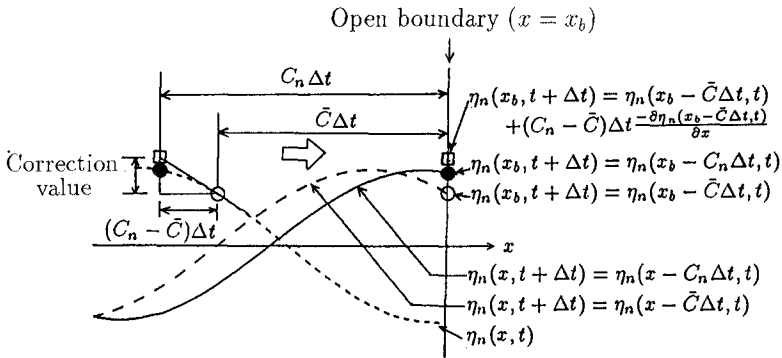

Fig.4: Physical interpretation of the improved Sommerfeld–type boundary condition for the one–dimensional case

The first term on the right–hand side of equation (10) expresses that the water

surface elevation of the wave at time t and at a point which is $\bar{C}\Delta t$ away from the outer edge of the energy absorbing layer is equal to that at the outer edge after Δt, because the wave moves to the outer edge. $\bar{C}$ is the wave celerity at the representative angular frequency, however, the wave celerity of irregular waves is different from $\bar{C}$. This is because irregular waves consist of many component waves with various angular frequencies. The second term on the right–hand side is a correction for the phase of the water surface elevation at the outer edge of the absorbing layer due to the difference in wave celerity.

Equation(10) is derived as follows. First we have

$$\eta(x_b, t + \Delta t) = \eta_n(x_b - \bar{C}\Delta t, t) - (C_n - \bar{C})\Delta t\frac{\partial\eta(x_b - \bar{C}\Delta t, t)}{\partial x} \qquad (11)$$

Expanding C_n into a Taylor series of $\Delta\omega_n$ and truncating the series at the first order gives

$$C_n = \bar{C} + \left(\frac{\overline{dC}}{d\omega}\right)\Delta\omega_n \qquad (12)$$

where $\left(\frac{\overline{dC}}{d\omega}\right)$ and $\Delta\omega_n$ are written as

$$\left(\frac{\overline{dC}}{d\omega}\right) = \frac{1}{\bar{k}}\left(1 - \frac{1}{\bar{n}}\right) \qquad (13)$$

$$\Delta\omega_n = \left(\frac{\overline{d\omega}}{dk}\right)\Delta k_n = \bar{n}\bar{C}\Delta k_n \qquad (14)$$

Next, we assume that $\eta_n(x, t)$ in equation (11) is expressed as $\eta_n(x, t) = a_n e^{i(k_n x - \omega_n t)}$ and differentiate $\eta_n(x, t)$ with respect to x. Expanding k_n in $\eta_n(x, t)$ into a Taylor series and truncating it at the first order gives

$$\frac{\partial\eta_n(x - \bar{C}\Delta t, t)}{\partial x} = i(\bar{k} + \Delta k_n)\eta_n(x - \bar{C}\Delta t, t) \qquad (15)$$

Substituting equations (12) to (15) into the second term of equation (11) and neglecting second–order terms of the resulting equation yield

$$-(C_n - \bar{C})\Delta t\frac{\partial\eta_n(x - \bar{C}\Delta t, t)}{\partial x} = i\bar{C}(1 - \bar{n})\Delta t\Delta k_n\eta_n(x - \bar{C}\Delta t, t) \qquad (16)$$

Equation (15) is rewritten as

$$i\Delta k_n\eta_n(x - \bar{C}\Delta t, t) = \frac{\partial\eta_n(x - \bar{C}\Delta t, t)}{\partial x} - i\bar{k}\eta_n(x - \bar{C}\Delta t, t) \qquad (17)$$

Substituting equation (17) into equation (16) gives

$$-(C_n - \bar{C})\Delta t\frac{\partial\eta_n(x - \bar{C}\Delta t, t)}{\partial x}$$
$$= \bar{C}(1 - \bar{n})\Delta t\left(\frac{\partial\eta_n(x - \bar{C}\Delta t, t)}{\partial x} - i\bar{k}\eta_n(x - \bar{C}\Delta t, t)\right) \qquad (18)$$

Equation (18) consists only of coefficients that are independent of the frequency and hence determined only by the representative frequency. Superposition of equation (18) for an infinite number of component waves gives the second term on the right–hand side of equation (10). The present open boundary condition combines equation (10) and the energy absorbing layer where the energy absorbing coefficient f_D is increased linearly towards the outer edge of the layer in the same way as Ohyama et $al.$ (1990).

In the present study, we determine the width of the energy absorbing layer and the coefficients $\bar{C}$, $\bar{n}$, and $\bar{k}$ in equation (10) as follows. The width is given as $0.6L_1$, where L_1 is the longest wavelength in the irregular waves. This width is chosen because reflection due to friction of the energy absorbing layer begins to increase rapidly at a width of $0.6L$ for a regular wave with wavelength L as obtained from the numerical calculations. Moreover, the coefficients $\bar{C}$, $\bar{n}$, and $\bar{k}$ in equation (10) are determined from the component wave having the longest wavelength. The energy absorption in the layer is the lowest for this component wave, implying that the energy at the outer edge of the layer is the highest. The behavior of the open boundary condition is shown in Figure 5. f_{Dmax} is the
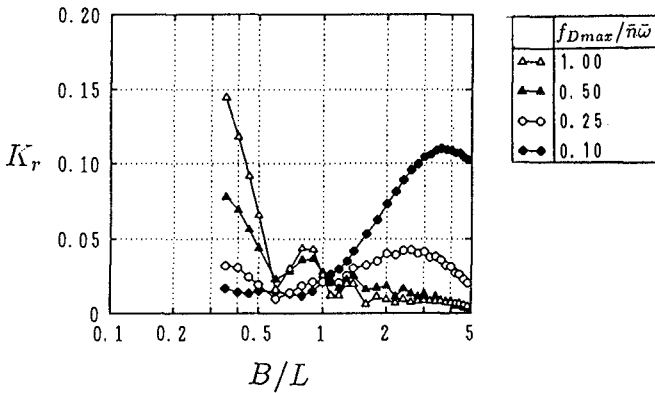

	$f_{Dmax}/\bar{n}\bar{\omega}$
△—△	1.00
▲—▲	0.50
○—○	0.25
●—●	0.10

Fig.5: Reflection coefficient for the improved open boundary condition in the one–dimensional case

maximum value of the energy absorbing coefficient, given at the outer edge of the layer. Figure 5 displays the reflection coefficient for component waves in an irregular wave field at a water depth of 10m that has a representative period of 6s and a longest period of 12s. It is seen that if B/L is greater than 0.6 and a proper value of f_{Dmax} is selected, the reflection coefficient becomes sufficiently small. The

previous method needed a width of $2L$ for a regular wave of wavelength L. Thus, a significant improvement is achieved with the present method.

4.2 Two–dimensional open boundary condition

In the horizontal two–dimensional case, it is necessary to approximate both the wave angle and the angular frequency by expanding them in Taylor series. For the two–dimensional case, equation (10) is written

$$
\begin{aligned}
&\eta_n(x, y, t + \Delta t) \\
= \ &\eta_n(x - \bar{C}\Delta t \cos \theta_n, y - \bar{C}\Delta t \sin \theta_n, t) \\
&+ \bar{C}(1 - \bar{n})\Delta t \cos \theta_n \frac{\partial \eta_n(x - \bar{C}\Delta t \cos \theta_n, y - \bar{C}\Delta t \sin \theta_n, t)}{\partial x} \\
&+ \bar{C}(1 - \bar{n})\Delta t \sin \theta_n \frac{\partial \eta_n(x - \bar{C}\Delta t \cos \theta_n, y - \bar{C}\Delta t \sin \theta_n, t)}{\partial y} \\
&- i\bar{C}(1 - \bar{n})\Delta t \bar{k} \eta_n(x - \bar{C}\Delta t \cos \theta_n, y - \bar{C}\Delta t \sin \theta_n, t)
\end{aligned}
\tag{19}
$$

The wave angle θ_n is expressed as the sum of a representative angle $\bar{\theta}$ and a deviation $\Delta \theta_n$:

$$
\theta_n = \bar{\theta} + \Delta \theta_n
\tag{20}
$$

We then substitute equation (20) into equation (19) and apply the additional theorem. Neglecting second order terms gives

$$
\Delta t \cos \theta_n = \Delta t \cos \bar{\theta}
\tag{21}
$$

$$
\Delta t \sin \theta_n = \Delta t \sin \bar{\theta}
\tag{22}
$$

Substituting equations (21) and (22) into equation (19) gives an equation in which the coefficients are independent of component angular frequencies and wave angles. Superimposing the equation gives an improved Sommerfeld–type boundary condition for the two–dimensional case.

$$
\begin{aligned}
&\eta(x, y, t + \Delta t) \\
= \ &\eta(x - \bar{C}\Delta t \cos \bar{\theta}, y - \bar{C}\Delta t \sin \bar{\theta}, t) \\
&+ \bar{C}(1 - \bar{n})\Delta t \cos \bar{\theta} \frac{\partial \eta(x - \bar{C}\Delta t \cos \bar{\theta}, y - \bar{C}\Delta t \sin \bar{\theta}, t)}{\partial x} \\
&+ \bar{C}(1 - \bar{n})\Delta t \sin \bar{\theta} \frac{\partial \eta(x - \bar{C}\Delta t \cos \bar{\theta}, y - \bar{C}\Delta t \sin \bar{\theta}, t)}{\partial y} \\
&- i\bar{C}(1 - \bar{n})\Delta t \bar{k} \eta(x - \bar{C}\Delta t \cos \bar{\theta}, y - \bar{C}\Delta t \sin \bar{\theta}, t)
\end{aligned}
\tag{23}
$$

where the representative wave angle $\bar{\theta}$ is determined from the gradient of the water surface elevation in the x and y directions at the outer edge of the energy-absorbing layer :

$$\bar{\theta} = \tan^{-1}\left(\frac{\partial\eta(x,y,t)/\partial y}{\partial\eta(x,y,t)/\partial x}\right) \qquad (24)$$

5   Calculation of wave field, nearshore current and bottom topography change

With the boundary conditions developed above, we carried out the calculation of deformation of multi–directional irregular waves around a detached breakwater on a uniform slope. The waves consisted of 958 components and were given by the single summation method. Also, the nearshore current and the bottom topography change were calculated by using the results of the calculation of the wave field. These results were compared with calculations for regular waves.

The method of calculating the nearshore current and the bottom topography change was similar to that of Kubo *et al.* (1992). Figure 6 shows the distribution of wave height for multi–directional irregular waves ($(H_{1/3})_0 = 1$m, $T_{1/3} = 6$s, $(\theta_p)_0 = 0$ °) around the breakwater, and Figure 7 shows the distribution for regular waves ($H_0 = 0.706$m, $T = 6$s) which has the same wave energy as the irregular waves. In the results for regular waves, a node and antinode occur in front of the detached breakwater, but for the multi–directional irregular waves, the variation in the wave height is small except just in front of the breakwater. This is because the multi–directional irregular waves consist of component waves with various wave direction and frequency, which affects the position of the node and antinode. Furthermore, the unreasonable value on the wave height due to the statistical variation that can be seen in the front of the breakwater in the results of Kubo *et al.* (1992) does not appear in the results of the present study. Figures 8 and 9 show the calculation results for the nearshore current under the above wave field. Overall, the current shows almost the same tendency, but the current velocity due to the multi–directional irregular waves is smaller than that due to the regular waves. This is because the radiation stress gradients become smaller around the average break point due to the variability in the break–point location and the large width of the surf zone for multi–directional irregular waves. In addition, in front of the breakwater the variation in the wave height, and hence the radiation stress, is large, however, a current does not occur since the gradients of the radiation stress and the mean water level are balanced here. Figure 10 shows the result of the calculation of the bottom topography change after 24 hours, computed by using the wave field in Figure 6 and the nearshore current
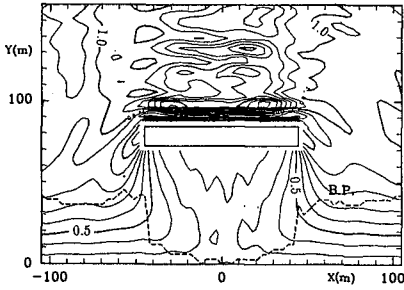
Fig.6: Wave height distribution
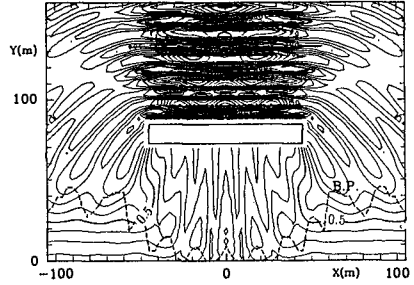(Multi-directional irregular waves)

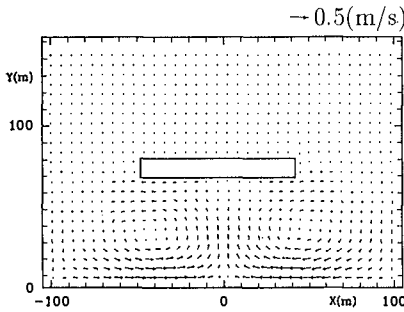Fig.7: Wave height distribution
(Regular waves)

Fig.8: Velocity distribution of
nearshore current
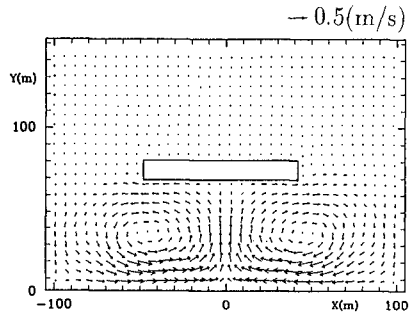(Multi-directional irregular waves)

Fig.9: Velocity distribution of
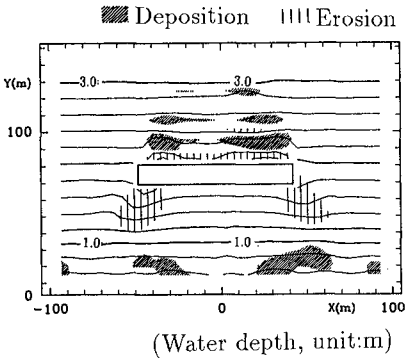nearshore current
(Regular waves)

(Water depth, unit:m)

Fig.10: Bottom topography change
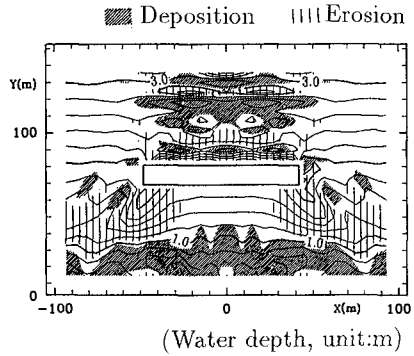(Multi-directional irregular waves)

(Water depth, unit:m)

Fig.11: Bottom topography change
(Regular waves)

field in Figure 8 as a steady external force. Figure 11 shows the result of the calculation of the bottom topography change after 24 hours for regular waves. By comparing these two figures, it is seen that the bottom topography change due to multi–directional irregular waves is smaller than that caused by regular waves with equal energy. This is because the bottom wave velocity and nearshore current are smaller for the multi–directional irregular waves.

6   Conclusion

A new incident wave boundary condition which is more efficient than that proposed previously is presented. In addition, the width of the energy absorbing layer is reduced by improving the non-reflective boundary condition for irregular waves. As a result, the accuracy in predicting the wave height distribution was considerably improved by reducing the statistical variation of the wave characteristics. The numerical model developed was applied to calculate the wave field, nearshore current and bottom topography change around a detached breakwater on a uniform slope. The results from calculations with regular and irregular waves were compared.

Acknowledgement

References

Berkhoff, J. C. W.(1972) : Computation of combined refraction–diffraction, Proc. 13th Int. Conf. on Coastal Eng., pp. 191-203.

Kotake, Y., M. Isobe and A. Watanabe (1992): On the high–order time–dependent mild–slope equation for irregular waves, Proc. 39th Japanese Conf. on Coastal Eng., pp. 91-95 (in Japanese).

Kubo, Y., Y. Kotake, M. Isobe and A. Watanabe (1992) : Time–dependent mild–slope equation for random waves, Proc. 23rd Int. Conf. on Coastal Eng., ASCE, pp. 419-431.

Ohyama, T. and N. Nadaoka (1990) : Modeling the transformation of nonlinear waves passing over a submerged step, Proc. Japanese Conf. on Coastal Eng., JSCE, Vol. 37, pp. 16-20 (in Japanese).